Current Biology 22, 945–955, June 5, 2012 ©2012 Elsevier Ltd All rights reserved DOI 10.1016/j.cub.2012.03.067

Article

# Raf Inhibitors Target Ras Spatiotemporal Dynamics

Kwang-jin Cho,[1] Rinshi S. Kasai,[2] Jin-Hee Park,[1] Sravanthi Chigurupati,[1] Sonja J. Heidorn,[4] Dharini van der Hoeven,[1] Sarah J. Plowman,[1] Akihiro Kusumi,[2,3] Richard Marais,[4,*] and John F. Hancock[1,*]
[1]Department of Integrative Biology and Pharmacology, The University of Texas Medical School–Houston, 6431 Fannin Street, Houston, TX 77030, USA
[2]Institute for Frontier Medical Sciences
[3]Institute for Integrated Cell-Material Sciences (WPI-iCeMS) Kyoto University, Kyoto 606-8507, Japan
[4]Signal Transduction Team, Section of Cell and Molecular Biology, Institute for Cancer Research, 237 Fulham Road, London SW3 6JB, UK

## Summary

**Background:** The lateral segregation of Ras proteins into transient plasma membrane nanoclusters is essential for high-fidelity signal transmission by the Ras mitogen-activated protein kinase (MAPK) cascade. In this spatially constrained signaling system, the dynamics of Ras nanocluster assembly and disassembly control MAPK signal output.
**Results:** We show here that BRaf inhibitors paradoxically activate CRaf and MAPK signaling in Ras transformed cells by profoundly dysregulating Ras nanocluster dynamics. Specifically, BRaf inhibitors selectively enhance the plasma membrane nanoclustering of oncogenic K-Ras and N-Ras but have no effect on H-Ras nanoclustering. Raf inhibitors are known to drive the formation of stable BRaf-CRaf and CRaf-CRaf dimers. Our results demonstrate that the presence of two Ras-binding domains in a single Raf dimer is sufficient and required to increase Ras nanoclustering, indicating that Raf dimers promote K- and N-Ras nanocluster formation by crosslinking constituent Ras proteins. Ras crosslinking increases the fraction of K-Ras and N-Ras in their cognate nanoclusters, leading to an increase in MAPK output from the plasma membrane. Intriguingly, increased MAPK signaling in BRaf inhibited cells is accompanied by significantly decreased Akt activation. We show that this signal pathway crosstalk results from a novel mechanism of competition between stabilized Raf dimers and p110α for recruitment to Ras nanoclusters.
**Conclusions:** Our findings reveal that BRaf inhibitors disrupt Ras nanocluster dynamics with significant, yet divergent, consequences for MAPK and PI3K signaling.

## Introduction

The plasma membrane is a dynamic, laterally heterogeneous structure that confers nonrandom spatial distributions on proteins in different types of transient yet functional nanoscale domains [1–5]. Understanding the underlying mechanisms that govern plasma membrane nanostructure is important because critical emergent properties can result from the spatial organization of signaling molecules. For example, the spatial organization of Ras proteins into plasma membrane nanoclusters is essential for high-fidelity signal transmission by the Ras-MAPK (mitogen-activated protein kinase) cascade [3, 6–8]. Ras guanosine triphosphate (GTP) nanoclusters are small (<20 nm in diameter), contain ~7 Ras proteins, and are the exclusive sites of Raf recruitment and ERK activation on the plasma membrane [3, 6, 8]. Raf activation within, and MAPK output from, an active Ras nanocluster is limited by the short (<1 s) lifetime of the cluster because disassembly of the nanocluster terminates signal output [3, 7, 8]. In this spatially constrained signaling system, the fraction of Ras proteins that assemble into nanoclusters and the lifetime of the nanocluster become important system parameters that determine MAPK responsiveness [3, 6–8]. Assessment of the importance of these system parameters has been limited to MAPK activation in model experimental cell systems, and the possible broader implications of modulating Ras nanoclustering has not been examined.

The discovery of BRaf as a frequent target for mutation in human tumors has driven the development of BRaf kinase inhibitors that have had marked clinical success in tumors such as melanoma [9–11]. In cells transformed by oncogenic mutant BRafV600E, ATP-competitive BRaf inhibitors abrogate ERK activation; however, in cells transformed by oncogenic mutant K- or N-Ras, these same inhibitors drive paradoxical MAPK activation in a CRaf-dependent manner [12–14]. Blocking BRaf activity using chemical inhibitors, or by mutation, drives kinase domain dimerization with CRaf and is permissive for CRaf activation [12, 13]. CRaf homodimerization is also promoted if the inhibitor binds to one CRaf protein in the dimer, to permit transactivation of the nonliganded CRaf protein [14]. Raf dimerization is essential for activation of the MAPK cascade because point mutations, which block Raf dimerization, prevent inhibitor-induced ERK activation [13, 14]. In cells expressing oncogenic Ras, BRaf inhibitors induce enhanced Ras-dependent translocation of wild-type (WT) BRaf and CRaf to the plasma membrane [12, 13]. Enhanced plasma membrane localization of CRaf in turn correlates closely with CRaf and MAPK activation [12–14]. Taken together, these studies clearly demonstrate that Ras is required to translate BRaf-CRaf or CRaf-CRaf dimerization into MAPK activation in intact cells, but the molecular role of Ras on the plasma membrane has not been elucidated.

In this study we examined whether Raf inhibitors perturb Ras spatiotemporal dynamics and show for the first time that induced changes to the emergent properties of Ras nanoclusters fully account for the observed effects of Raf inhibitors on Ras signal transmission.

## Results

### Raf Inhibition Stimulates Oncogenic K-Ras and N-Ras Nanoclustering on the Plasma Membrane

Several studies have reported that treatment of oncogenic mutant Ras transformed cells with BRaf inhibitors significantly enhances the plasma membrane recruitment of CRaf [12, 13, 15]. Because Ras.GTP nanoclusters are the sites of Raf recruitment to the plasma membrane [3, 6, 8], these observations

*Correspondence: richard.marais@icr.ac.uk (R.M.), john.f.hancock@uth.tmc.edu (J.F.H.)

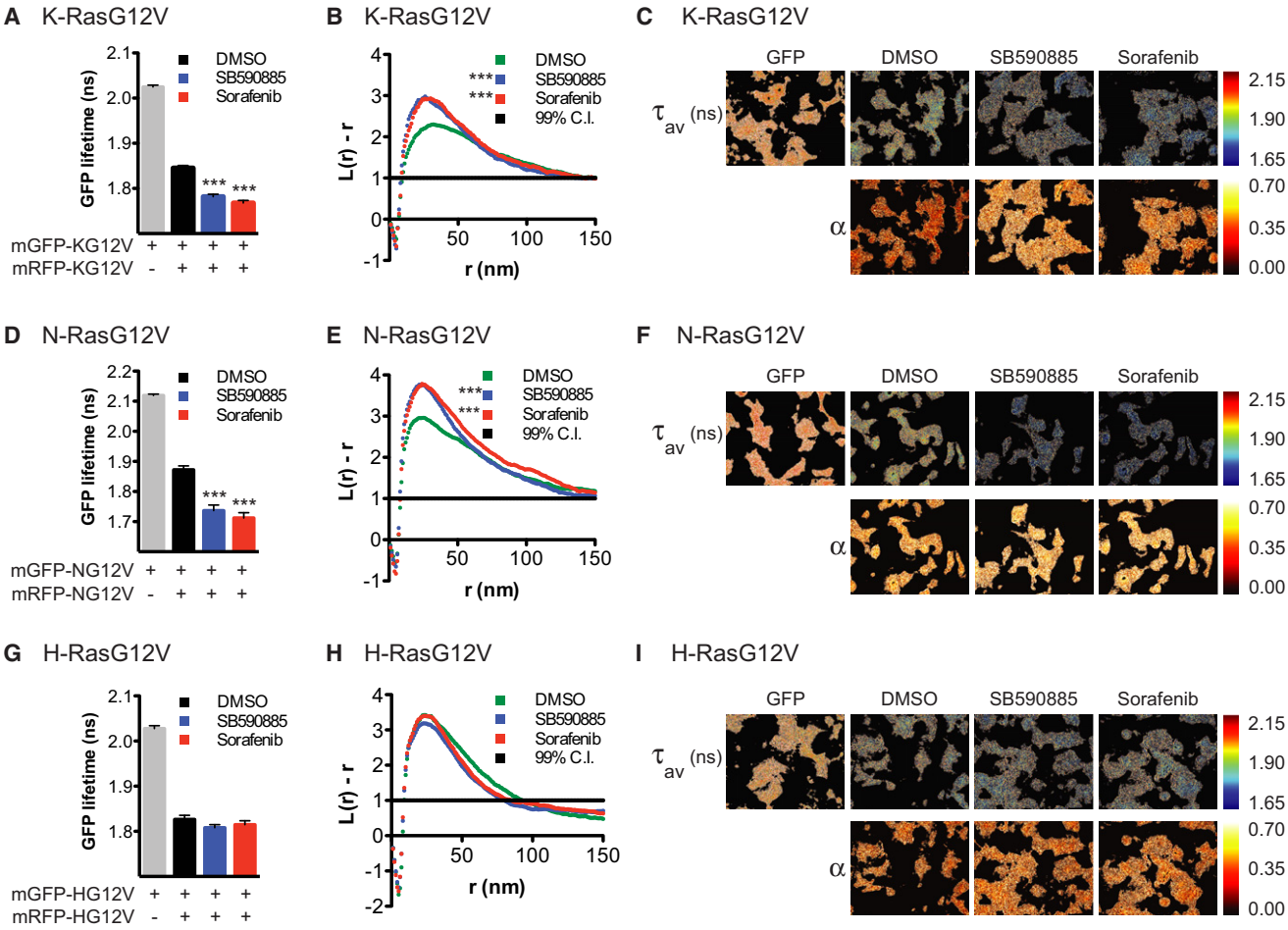


Figure 1. Raf Inhibition Enhances Oncogenic K-Ras and N-Ras Nanoclustering

(A, D, and G) BHK cells expressing mGFP- and mRFP-RasG12V were treated with Raf inhibitors (0.1 μM SB590885, 10 μM sorafenib) for 4 hr, and the lifetime of GFP measured using a FLIM-microscope. The graph shows mean fluorescence lifetime of GFP ± SEM (n ≥ 102 cells, from three independent experiments). Significant differences between Raf inhibitor-treated and control (DMSO-treated) cells were assessed using one-way ANOVA tests (***p < 0.001).

(C, F, and I) Representative pseudocolored images showing average GFP fluorescence lifetime ($\tau_{av}$) in nanoseconds and the mGFP-RasG12V FRET fraction (α). The image labeled GFP is from cells expressing mGFP-RasG12V only; the other images are from cells coexpressing mGFP- and mRFP-RasG12V. Treatment with Raf inhibitors had no effect on mGFP-RasG12V lifetime in cells not expressing a FRET acceptor (Figure S1).

(B, E, and H) Intact plasma membrane sheets prepared from BHK cells expressing mGFP-RasG12V and treated for 4 hr with Raf inhibitors (0.1 μM SB590885, 10 μM sorafenib) were immunogold labeled. Spatial mapping of the gold-labeled Ras distribution was performed for each experimental condition. The *L(r) – r* curve is a weighted mean K function (n ≥ 15), where values above the 99% C.I. for a random pattern indicate clustering at that value of *r*. Significant differences between the *L(r) – r* curves of Raf inhibitor-treated and control (DMSO treated) cells were evaluated in bootstrap tests (***p < 0.001). Sample micrographs are shown in Figure S1.

strongly suggested that BRaf inhibitors might increase the fraction of oncogenic Ras proteins that assemble into nanoclusters. To examine the effect of blocking Raf kinase activity on Ras nanoclustering, we treated baby hamster kidney (BHK) cells transiently coexpressing mGFP- and mRFP-tagged oncogenic K-RasG12V (KG12V) with the BRaf inhibitor SB590885 or the BRaf and CRaf inhibitor sorafenib [16, 17]. Nanoclustering was assayed by measuring mGFP fluorescence lifetime using a fluorescence-lifetime imaging microscopy (FLIM) microscope. In untreated control cells, coexpression of mGFP-KG12V and mRFP-KG12V significantly decreased mGFP fluorescence lifetime, indicating fluorescence resonance energy transfer (FRET) between mGFP-KG12V and mRFP-KG12V molecules. This result is consistent with previous results showing that a fraction (~40%) of KG12V proteins are arrayed in nanoclusters on the plasma membrane [3, 8]. Treatment with SB590885 or sorafenib induced further reductions in mGFP-KG12V fluorescence lifetime (Figures 1A and 1C). These reductions in mGFP fluorescence lifetime were a consequence of a substantial increase in the fraction of mGFP-KG12V molecules undergoing FRET in the BRaf inhibited cells (see Table S1A available online). These results indicate that Raf inhibition significantly increases KG12V nanoclustering. To validate this conclusion, we prepared intact 2D plasma membrane sheets from BHK cells expressing mGFP-KG12V and labeled with anti-GFP antibody conjugated directly to 5 nm gold particles. Images of the gold particles were taken using an electron microscope (EM) and the spatial organization of mGFP-KG12V was analyzed using Ripley's K-function (Figure 1B). The *L(r) – r* plots show that mGFP-KG12V is clustered in control cells but that mGFP-KG12V clustering is significantly increased when cells are

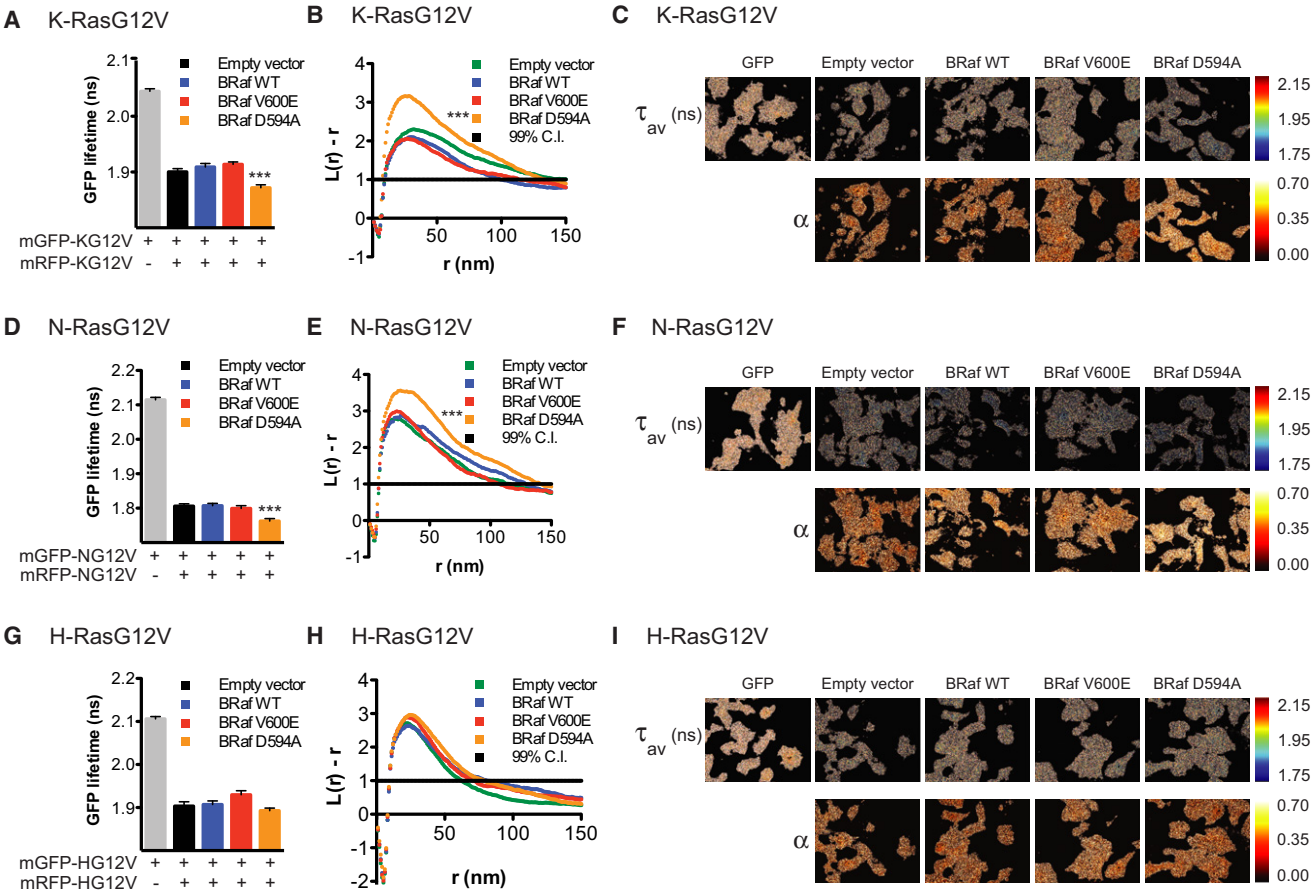


Figure 2. Kinase-Dead BRaf Enhances Oncogenic K-Ras and N-Ras Nanoclustering

(A, D, and G) BHK cells were cotransfected with BRaf constructs in the presence of mGFP- and mRFP- RasG12V, and the fluorescence lifetime of GFP measured using a FLIM-microscope. The graph shows mean fluorescence lifetime of GFP ± SEM (n ≥ 95 cells, from three independent experiments). Significant differences between BRaf-transfected and empty vector-transfected cells were assessed using one-way ANOVA tests (***p < 0.001).

(C, F, and I) Representative pseudocolored images showing average GFP fluorescence lifetime ($\tau_{av}$) in nanoseconds and the mGFP-RasG12V FRET fraction ($\alpha$). The image labeled GFP is from cells expressing mGFP-RasG12V only; the other images are from cells coexpressing mGFP- and mRFP-RasG12V.

(B, E, and H) Intact plasma membrane sheets were prepared from BHK cells expressing mGFP-RasG12V and BRaf constructs and immunogold labeled. Spatial mapping of the gold-labeled Ras distribution was performed for each experimental condition. The *L(r) – r* curve is a weighted mean K-function (n ≥ 15), where values above the 99% C.I. for a random pattern indicate clustering at that value of *r*. Significant differences between the *L(r) – r* curves of BRaf-transfected and empty vector-transfected cells were evaluated in bootstrap tests (***p < 0.001).

treated with sorafenib or SB590885. Further interrogation of these spatial point patterns showed that the increase in *L(r) – r* values is accounted for by an increase in the mGFP-KG12V clustered fraction (Table S1A). Because the ability of different Ras isoforms to recruit Raf proteins to nanoclusters varies, we repeated these experiments with cells transformed by oncogenic N-RasG12V (NG12V) or oncogenic H-RasG12V (HG12V). The results show that SB590885 and sorafenib treatment significantly increased NG12V nanoclustering (Figures 1D–1F; Table S1B) but had no effect on HG12V nanoclustering (Figures 1G–1I; Table S1C).

Ectopic expression of kinase-dead BRaf in Ras transformed cells enhances MAPK activation as efficiently as treatment with SB590885 [12]. We therefore analyzed Ras spatial organization in cells coexpressing BRaf mutants. The FLIM-FRET and EM analyses in Figures 2A–2F show that ectopic expression of kinase-dead BRaf (D594A), but not WT or constitutively active BRaf (V600E), significantly increased KG12V and NG12V nanoclustering but had no effect on HG12V nanoclustering (Figures 2G–2I). These results are consistent with previous work showing that membrane-recruited CRaf is efficiently retained in KG12V but not HG12V nanoclusters [18]. Taken together, the data in Figures 1 and 2 and Table S1 show that BRaf inhibition significantly increases the nanoclustering of oncogenic K- and N-Ras on the plasma membrane.

### Ras-Binding Domains of B- and C-Raf Are Sufficient for Stimulating Oncogenic K-Ras and N-Ras Nanoclustering

The crosslinking of lipid raft domains by multivalent ligands or antibodies can stabilize these transient nanodomains and activate associated signaling complexes [19, 20]. We reasoned that a similar mechanism could operate in cells treated with BRaf inhibitors because the formation of stable CRaf-BRaf or CRaf-CRaf dimers [12–14], which have two Ras binding domains (RBDs), could potentially crosslink nanoclustered Ras proteins. We therefore generated a tandem RBD-CRD fusion protein (2×RBD-CRD) comprising the RBD and cysteine-rich domain (CRD) of BRaf and CRaf (Figure 3A) separated by a short flexible linker sequence. As a control, we introduced a point mutation at a critical arginine residue

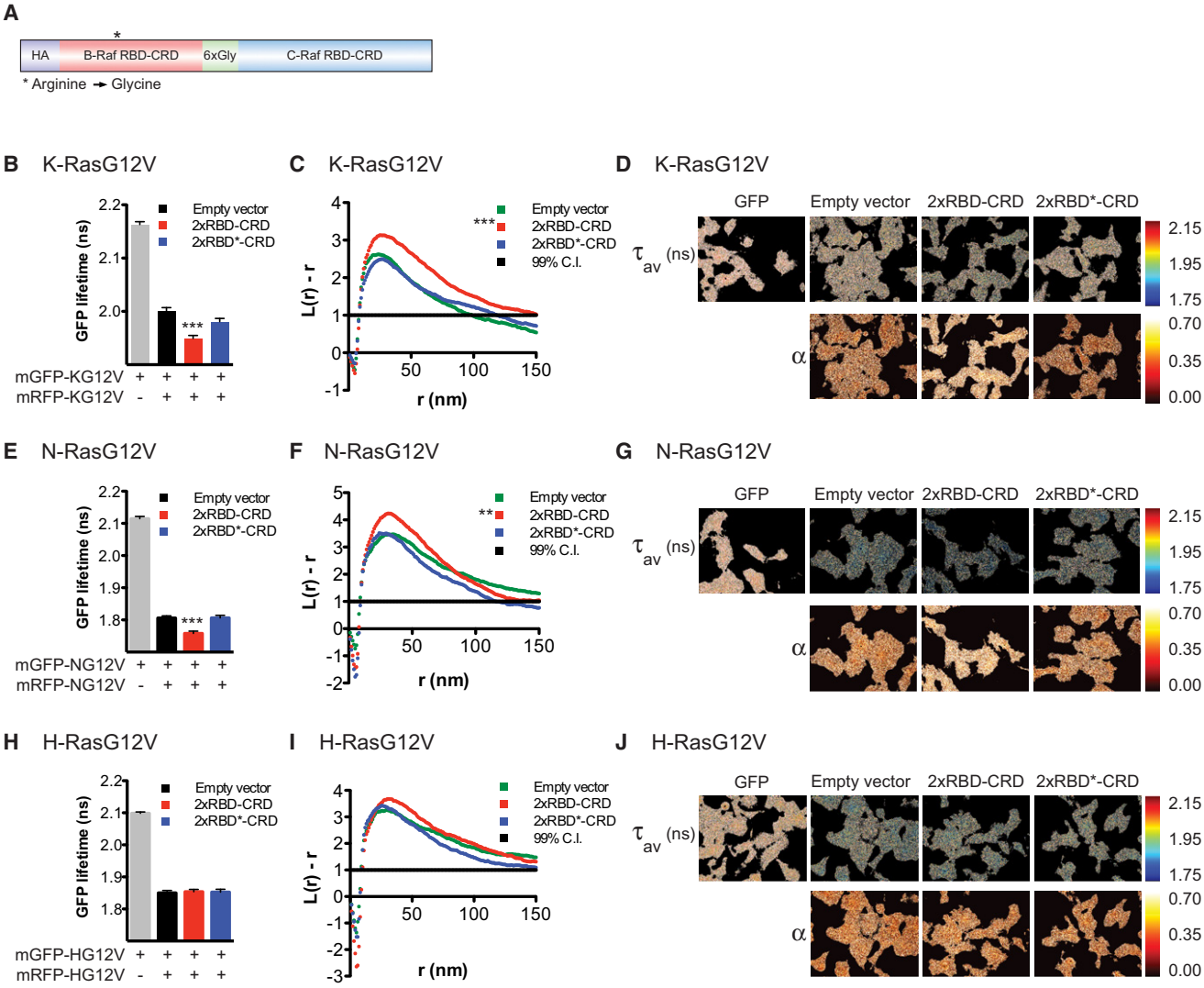


Figure 3. A Dimer of the RBD of CRaf and BRaf Is Sufficient to Enhance K-Ras and N-Ras Nanoclustering

(A) Diagram of the tandem RBD-CRD construct (2×RBD-CRD), comprising amino acids 150–300 of BRaf and amino acids 2–200 of CRaf joined by poly-Gly linker and appended with an N-terminal hemagglutinin epitope tag (HA). The 2×RBD*-CRD contains a R188G point mutation in the BRaf RBD sequence, which abrogates Ras binding.

(B, E, and H) BHK cells were cotransfected with tandem RBD-CRD constructs in the presence of mGFP- and mRFP-RasG12V, and the fluorescence lifetime of GFP was measured using a FLIM microscope. The graph shows mean fluorescence lifetime of GFP ± SEM ($n \geq 92$ cells, from three independent experiments). Significant differences between cells expressing tandem RBD-CRD constructs and empty vector were assessed using one-way ANOVA tests (***$p < 0.001$).

(D, G, and J) Representative pseudocolored images showing average GFP fluorescence lifetime ($\tau_{av}$) in nanoseconds and the mGFP-RasG12V FRET fraction ($\alpha$). The image labeled GFP is from cells expressing mGFP-RasG12V only; the other images are from cells coexpressing mGFP- and mRFP-RasG12V.

(C, F, and I) Intact plasma membrane sheets were prepared from BHK cells expressing mGFP-RasG12V and tandem RBD-CRD constructs and immunogold labeled. Spatial mapping of the gold-labeled Ras distribution was performed for each experimental condition. The *L(r) – r* curve is a weighted mean K-function ($n \geq 15$), where values above the 99% C.I. for a random pattern indicate clustering at that value of *r*. Significant differences between the *L(r) – r* curves of tandem RBD-CRD constructs and empty vector-transfected cells were evaluated in bootstrap tests (***$p < 0.001$ or **$p < 0.01$). See also Figure S2.

in the BRaf RBD (2×RBD*-CRD), which abrogates Ras binding [21]. FLIM-FRET imaging and EM spatial analysis showed that ectopic expression of 2×RBD-CRD, but not 2×RBD*-CRD, significantly increased the nanoclustering of KG12V and NG12V (Figures 3B–3G; Tables S1A and S1B). Ectopic expression of 2×RBD-CRD had no effect on the extent of HG12V nanoclustering (Figures 3H–3J; Table S1C), consistent with the results in Figures 1 and 2. We generated additional tandem RBD-CRD fusion proteins to simulate CRaf-CRaf and BRaf-BRaf homodimers; both of these homodimeric Raf fusion proteins increased the nanoclustering of NG12V and KG12V but had no effect on HG12V nanoclustering (Figure S3). As with the 2×RBD*-CRD construct, a point mutation in a single RBD abolished the ability of the homodimeric Raf fusion proteins to increase Ras nanoclustering (Figure S3). Taken together, these data indicate that two RBDs must be simultaneously available in a single Raf homo- or heterodimer to enhance K-Ras.GTP or N-Ras.GTP nanoclustering and suggest that crosslinking Ras.GTP proteins is the underlying molecular mechanism that stabilizes Ras nanoclusters.

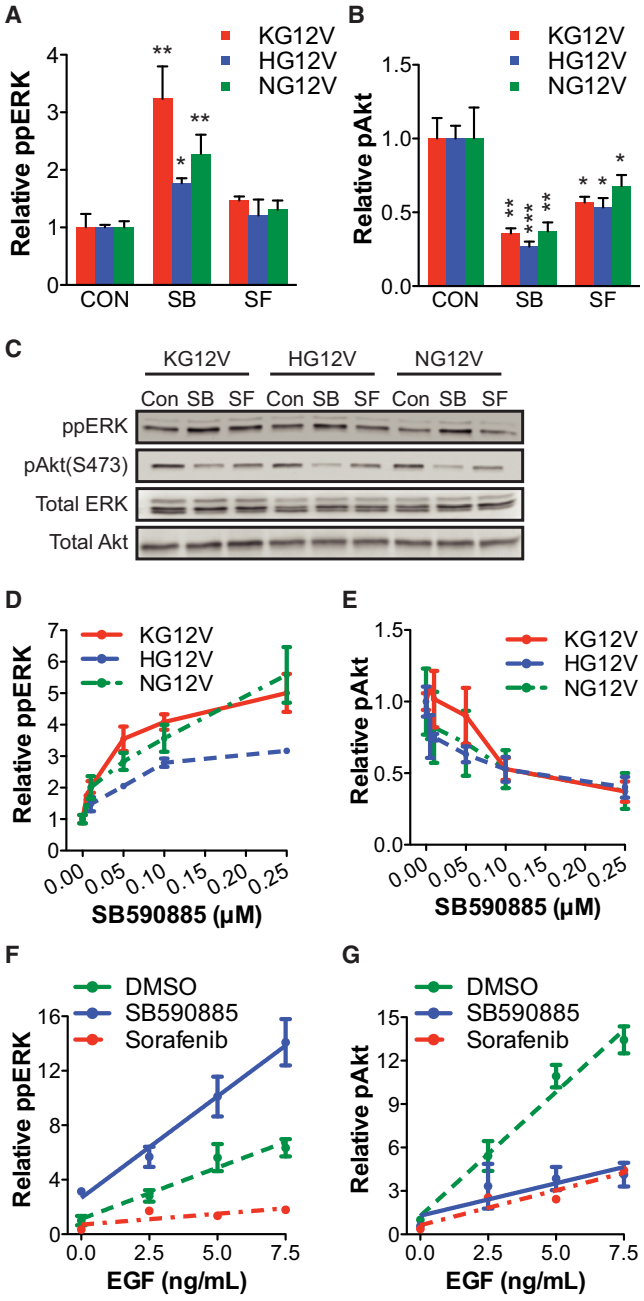


Figure 4. BRaf Inhibition Activates ERK but Reduces Akt Phosphorylation

BHK cells stably expressing oncogenic Ras isoforms were treated with Raf inhibitors (0.1 μM SB590885, 10 μM sorafenib) for 4 hr, and cell lysates immunoblotted for ppERK and pAkt (S473). The graphs show mean ppERK (A) and mean pAkt levels ± SEM (n = 3) (B) relative to the respective control (DMSO-treated) treated RasG12V cell line. (Con, control [DMSO]; SB, SB590885; and SF, sorafenib). Significant differences between control and Raf inhibitor-treated cells were assessed using one-way ANOVA tests (**$p < 0.01$ or *$p < 0.05$). A representative blot is shown (C) (Con, control [DMSO]; SB, SB590885; and SF, sorafenib). Serum starved BHK cells stably expressing oncogenic Ras isoforms were treated for 2 hr with SB590885. Cell lysates were immunoblotted for ppERK and pAkt(S473). The graphs show mean ppERK (D), and mean pAkt levels ± SEM (n = 3) (E) relative to respective control RasG12V cells lines. A representative blot is shown in Figure S3. Untransfected serum starved BHK cells were pretreated for 2 hr with Raf inhibitors (0.1 μM SB590885, 50 μM sorafenib) and stimulated for 2 min with EGF. Cell lysates were immunoblotted for ppERK and pAkt(S473). The graphs show mean ppERK (F), and mean pAkt levels ± SEM (n = 3) (G). A representative blot is shown in Figure S3.

Table S1 also shows that treatment with BRaf inhibitors or expression of kinase-dead BRaf (D594A) or 2×RBD-CRD, while not increasing the average number of Ras molecules per cluster, all increase FRET efficiency, suggesting that organization of K-Ras and N-Ras proteins within their cognate nanoclusters is altered as a result of Ras crosslinking.

Given the selective effect of BRaf inhibitors on the clustering of N- and K-Ras, we looked for isoform selective effects on signal transmission. BHK cells stably expressing oncogenic K-, N-, or H-Ras were treated with Raf inhibitors and ppERK and pAkt (S473) levels were measured. SB590885 induced significantly greater ERK activation in KG12V and NG12V cells than in HG12V cells (Figure 4A). Interestingly SB590885 also significantly reduced Akt phosphorylation in all three transformed cell lines (Figure 4B). The effects of SB590885 on stimulating activation of ERK and inhibiting activation of Akt in cells stably expressing oncogenic K-, N-, or H-Ras were dose-dependent (Figures 4D and 4E; Figures S3A and S3B). Sorafenib treatment had no detectable effect on ppERK levels in the KG12V, NG12V, and HG12V cells, unless used at high concentrations (Figure S3E), but as seen with SB590885, sorafenib significantly inhibited pAkt levels in all three Ras transformed cell lines. Similar effects of the Raf inhibitors were seen on a cohort of six human endometrial, lung, and breast cancer cell lines: SB590885, but not sorafenib, significantly stimulated ppERK level in all cancer cell lines tested (Figures S3F–S3I), with reciprocal inhibition of pAkt levels that was most marked in cells expressing oncogenic K-Ras (HEC-1a, A549, and MDA-MB-231) or constitutively active PI3K (ESS-1).

### Endogenous Ras Signaling Is Dysregulated by Raf Inhibitors

The spatiotemporal dynamics of Ras nanoclustering are critically important for high-fidelity signal transmission through the MAPK cascade. Our computational experiments indicate that increasing the fraction of Ras proteins that assemble into clusters increases the gain in the EGF-MAPK signaling pathway [3, 6, 7, 22, 23]. To assay for this effect, we preincubated BHK cells with SB590885 or sorafenib and stimulated for 2 min with nonsaturating doses of EGF. Stimulation times were kept short so that only plasma membrane signaling events were assayed [24–26] (Figures 4F and 4G; Figures S3C and S3D). Control cells and cells pretreated with SB590885 and sorafenib all showed linear ppERK dose responses to low dose EGF stimulation; however, the slope and magnitude of the ppERK response was substantially greater in SB590885-treated cells, consistent with increased signal gain. Sorafenib-treated cells showed a diminished EGF response presumably because concomitant blockade of CRaf kinase activity mitigates the potential enhanced ppERK activation flowing from enhanced nanoclustering (Figure 4F). Of note, however, both Raf inhibitors significantly reduced Akt phosphorylation in response to EGF stimulation (Figure 4G), as seen in cells transformed by oncogenic mutant Ras.

### Competition for Stabilized Ras Nanoclusters between Raf Dimers and PI3K

We consistently observed reduced Akt activation in cells treated with Raf inhibitors, suggesting molecular competition between dimerized Raf and PI3K for recruitment to Ras nanoclusters. To explore this mechanism, we treated BHK cells coexpressing RasG12V and BRaf or CRaf with Raf inhibitors and measured Ras-Raf interactions in intact cells using

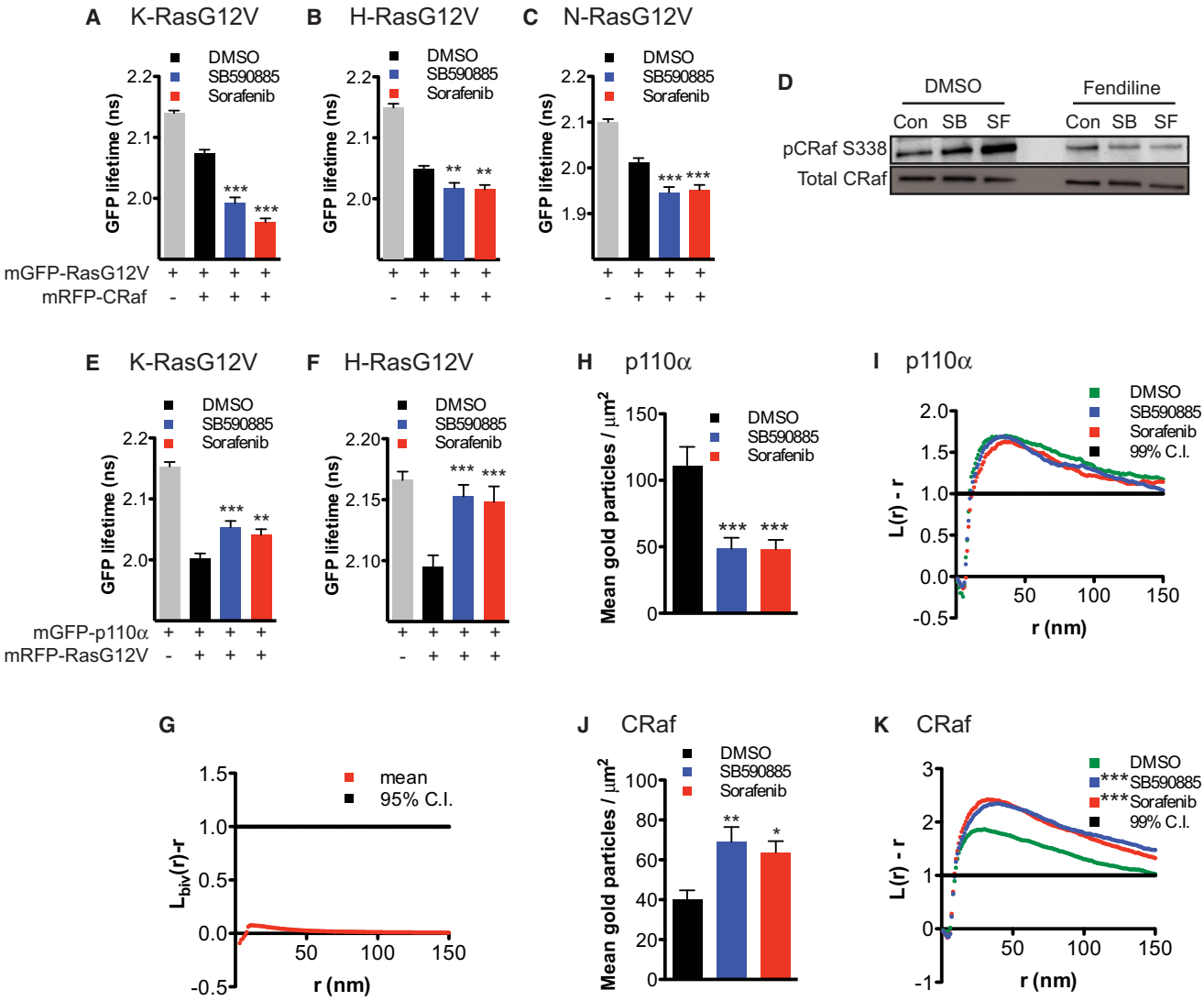


Figure 5. Competition for Stabilized Nanoclusters between Raf and PI3K

BHK cells expressing mGFP-CRaf or mGFP-p110α with mRFP-RasG12V were treated with Raf inhibitors (0.1 μM SB590885, 10 μM sorafenib) for 4 hr, and the fluorescence lifetime of GFP was measured in a FLIM microscope (A–C, E, and F). The graph shows mean fluorescence lifetime of GFP ± SEM ($n \geq 50$ cells, from three independent experiments). Significant differences between Raf inhibitor-treated and DMSO-treated cells were assessed using one-way ANOVA tests (***$p < 0.001$, **$p < 0.01$). BHK cells stably expressing mGFP-KG12V were treated with fendiline for 2 days and further incubated with Raf inhibitors (0.1 μM SB590885, 10 μM sorafenib) for 4 hr. Cell lysates were immunoblotted for CRaf-pS338, a phosphorylation site that correlates with Raf activity. A representative blot of three independent experiments is shown (D) (CON, DMSO treated control; SB, SB590885; and SF, sorafenib). Intact plasma membrane sheets were prepared from K-RasG12V transformed CHO cells expressing mGFP-p110α and mRFP-CRaf and immunogold labeled with 6 nm anti-GFP and 2 nm anti-RFP gold. (G) Spatial analysis was performed using a bivariate K-function that determines whether one gold population is clustered with respect to the other. The $L_{biv}(r) - r$ curve is a weighted mean bivariate K-function (n = 25), where values above the 95% C.I. for a random pattern indicate coclustering at that value of $r$. Intact plasma membrane sheetes prepared from K-RasG12V transformed CHO cells expressing mGFP-p110α (H) or mRFP–CRaf (J) and treated with Raf inhibitors (0.1 μM SB590885, 10 μM sorafenib) for 4 hr were immunogold labeled as in (G). Plasma membrane recruitment was assayed by counting gold particles: the graph shows the mean number of gold particles/$\mu m^2$ ± SEM ($n \geq 25$). Significant differences between Raf inhibitor-treated and control (DMSO-treated) cells were assessed using one-way ANOVA tests (***$p < 0.001$, **$p < 0.01$, or *$p < 0.05$). The individual gold distributions corresponding to mGFP-p110α (I) or mRFP–CRaf (K) were analyzed by univariate K-functions. Significant differences between Raf inhibitor-treated and control (DMSO-treated) $L(r) - r$ curves were evaluated in bootstrap tests (***$p < 0.001$). See also Figure S4.

FLIM-FRET imaging. The results show that the interactions of BRaf and CRaf with KG12V, NG12V, and HG12V were all increased in the presence of Raf inhibitors (Figures 5A–5C; Figures S4A–S4C). The increased interaction of Raf dimers with stabilized KG12V nanoclusters directly increases CRaf activation, as evidenced by significantly enhanced CRaf S338 phosphorylation in KG12V cells treated with sorafenib or SB590885 (Figure 5D). Cotreating cells with fendiline, which inhibits the plasma membrane interaction of K-Ras (J.F.H. and D.v.d.H., unpublished data), reversed CRaf activation by SB590885 or sorafenib (Figure 5D). Thus K-Ras must be localized specifically to the plasma membrane in order for dimerized Raf to undergo activation.

Next, BHK cells were cotransfected with mGFP-p110α and mRFP-KG12V or mRFP-HG12V, and mGFP fluorescence lifetime was used as a measure of RasG12V/p110α proximity.

FRET between mGFP-p110α and both mRFP-KG12V and mRFP-HG12V was significantly reduced when cells were treated Raf inhibitors (Figures 5E and 5F), suggesting that p110α interaction with KG12V and HG12V is indeed abrogated when Ras nanoclusters recruit BRaf-CRaf dimers. To confirm this interpretation, we used EM to spatially map p110α and CRaf distributions on the plasma membrane in the presence and absence of Raf inhibitors. Intact 2D plasma membrane sheets prepared from KG12V transformed Chinese hamster ovarian (CHO) cells coexpressing mGFP-p110α and mRFP-CRaf, were labeled with anti-GFP and anti-RFP antibodies conjugated directly to 6 or 2 nm gold particles, respectively. EM images of the gold particles were analyzed. The bivariate K-function, $L_{biv}(r) - r$, shows that mGFP-p110α and mRFP-CRaf do not cocluster (Figure 5G), definitive evidence that CRaf and PI3K proteins are not recruited to the same KG12V nanoclusters. Treatment with BRaf inhibitors however simultaneously reduced p110α levels and increased CRaf levels on the plasma membrane as evidenced by the reciprocal changes in labeling by 6 nm and 2 nm gold particles (Figures 5H and 5I). Univariate K-function analysis, $L(r) - r$, of the individual gold populations showed that p110α and CRaf proteins were both recruited to plasma membrane nanoclusters, but whereas the extent of p110α clustering did not change, the extent of CRaf clustering significantly increased on treatment with BRaf inhibitors (Figures 5J and 5K). These changes in clustering are not a consequence of different gold pattern densities, because the spatial analysis corrects for this parameter. Rather, taken together, the results show that when K-Ras.GTP (KG12V) nanoclusters are crosslinked by BRaf-CRaf dimers, the dimers are retained within the nanoclusters leading to increased Raf levels and increased Raf clustering. In consequence, fewer K-Ras.GTP (KG12V) nanoclusters are available for p110α recruitment and activation. This mechanism fully accounts for the reciprocal effects on MAPK and Akt activation in cells treated with BRaf inhibitors. Finally, we determined whether 2×RBD-CRD molecules, in contrast to p110α, could efficiently compete with signaling competent Raf dimers for access to Ras nanoclusters. Figures S4D and S4E show that KG12V nanoclustering in cells expressing 2×RBD-CRD was not further increased on treatment with SB90885; however, 2×RBD-CRD significantly reduced SB590885-stimulated MAPK activation in RasG12V cells.

### BRaf Inhibition Increases the Probability of K-Ras Nanocluster Formation

We have shown that BRaf inhibitors increase the fraction of K-Ras and N-Ras in nanoclusters on the plasma membrane. To explore the effect of Raf inhibitors on nanocluster dynamics, we used single fluorophore video tracking (SFVT). The diffusion of single Ras molecules on the plasma membrane is characterized by periods of free diffusion interspersed with periods of transient immobilization [27]; these transient immobilization periods (TIMPs) correlate with assembly of the Ras protein into a transient nanocluster [27, 28]. We therefore recorded and analyzed multiple trajectories of single mGFP-KG12V molecules expressed in BHK cells in the presence of SB590885, sorafenib, or dimethyl sulfoxide (DMSO) (control). Sample trajectory tracings are shown in Figure 6A, and representative movies of the trajectories are included in the Supplemental Information (Movies S1, S2, and S3). TIMP durations and the radii of confinement of the TIMPs were measured and are plotted as frequency histograms in Figure 6B. The radius of the TIMPs in these trajectories is similar to the radius of nanoclusters identified by EM, although the accuracies of the determined radii are quite limited due to the localization error of single fluorescent molecules (Figures 6B and 6C; Figure 1). The distributions of TIMP durations were fitted by single exponential decay functions to estimate decay constants (Figure 6B), which were corrected for the photobleaching lifetime of mGFP on the cell surface (Figure 6C). The summary results show that the overall time fraction of temporary immobilization of mGFP-KG12V increased significantly when cells were treated SB590885 or sorafenib (Figure 6C). This result qualitatively recapitulates the EM and FLIM results in Figure 1 that showed an increase in the Ras nanoclustered fraction. However, because SVFT tracking can only identify Ras interactions with nanoclusters that have a lifetime of >100 ms, we expect a higher clustered fraction estimate from EM and FLIM imaging that identifies all Ras nanoclusters (Table S1). Most interestingly, further analysis of the SFVT data showed that the significant increase in the time fraction of temporary immobilization is not due to a change in the average lifetime of the TIMPs but rather a reduced diffusing period between TIMPs, indicating an increase in TIMP frequency (Figure 6C). Taking the results together, we can conclude that BRaf inhibitor-induced Raf dimers cause an increase in the rate, or probability, of Ras nanocluster formation but do not actually prolong the lifetime of Ras nanoclusters once they are assembled.

## Discussion

Here we identify perturbation of Ras spatiotemporal dynamics as the mechanistic basis of paradoxical activation of the MAPK cascade by BRaf inhibitors [12–14, 29]. Specifically, we show that Raf heterodimerization induced by Raf inhibitors, or expression of kinase-dead BRaf, enhances the nanoclustering of oncogenic K-Ras and N-Ras, but not H-Ras. These effects are not limited to oncogenic Ras, because the nanoclustering of, and MAPK signal output from, WT Ras.GTP is also enhanced by BRaf inhibitors. Similar effects on oncogenic mutant Ras.GTP and WT Ras.GTP nanoclusters is to be expected because the assembly and disassembly of signaling Ras.GTP nanoclusters occur on a time scale of <1 s and is not linked to GTP hydrolysis [27, 28].

Our results show that two Raf RBDs must be simultaneously available in a single dimer to bind to Ras.GTP in order to enhance K-Ras.GTP and N-Ras.GTP nanoclustering. All Raf dimers tested—BRaf-BRaf, CRaf-CRaf, and BRaf-CRaf—were able to enhance Ras nanoclustering. We therefore envisage that the basic mechanism driving an increase in nanoclustering requires two RBDs in a Raf dimer that are able to transiently crosslink Ras.GTP proteins. SFVT experiments in live cells further show that Raf dimers increase the actual rate of formation of Ras nanoclusters. We speculate that the availability of crosslinking dimers at the time of collision between Ras monomers increases the probability of that collision leading to successful nanocluster assembly. In this sense, the dimer may operate as an additional bivalent nanocluster scaffold, similar to polyvalent galectin-3 that facilitates assembly of K-Ras nanoclusters [18, 30–32]. Once the Ras nanocluster has formed, the crosslinking activity of the Raf dimer does not actually prolong the lifetime of the resulting cluster.

Increasing the probability of nanocluster formation increases the Ras clustered fraction and therefore promotes MAPK activation. This follows because the fraction of Ras.GTP

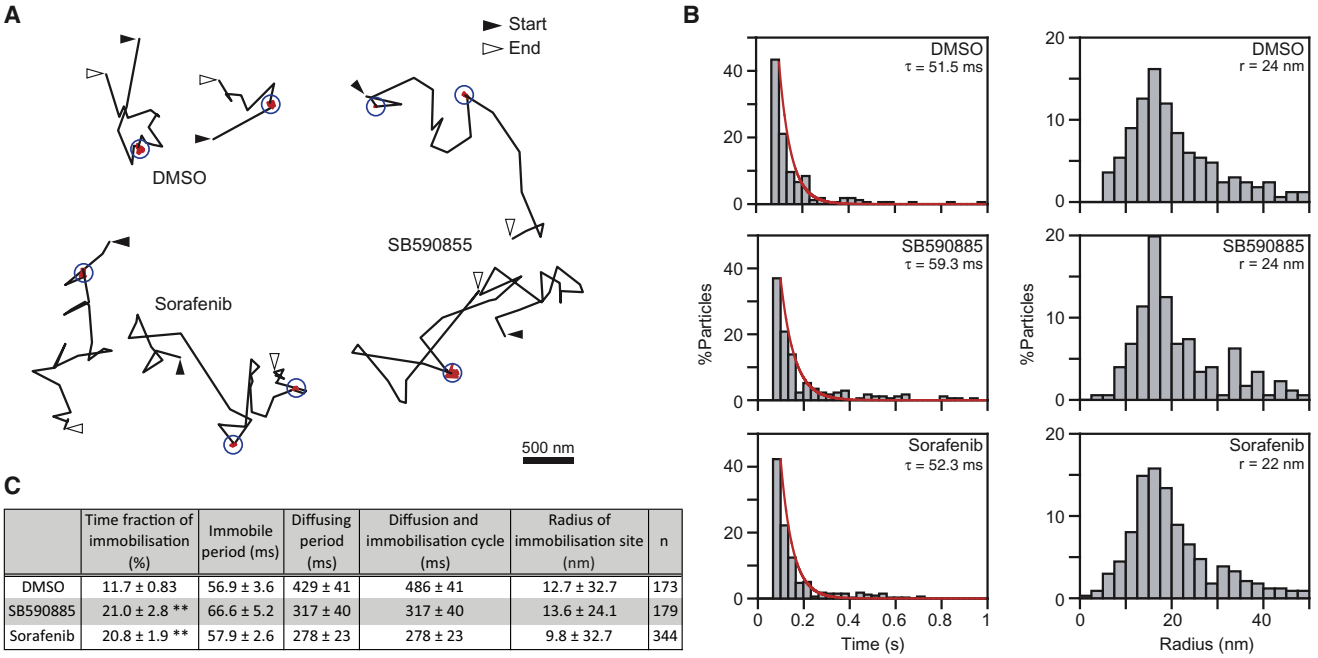


C

| | Time fraction of immobilisation (%) | Immobile period (ms) | Diffusing period (ms) | Diffusion and immobilisation cycle (ms) | Radius of immobilisation site (nm) | n |
|---|---|---|---|---|---|---|
| DMSO | 11.7 ± 0.83 | 56.9 ± 3.6 | 429 ± 41 | 486 ± 41 | 12.7 ± 32.7 | 173 |
| SB590885 | 21.0 ± 2.8 ** | 66.6 ± 5.2 | 317 ± 40 | 317 ± 40 | 13.6 ± 24.1 | 179 |
| Sorafenib | 20.8 ± 1.9 ** | 57.9 ± 2.6 | 278 ± 23 | 278 ± 23 | 9.8 ± 32.7 | 344 |

Figure 6. Raf Inhibitors Enhance the Probability of K-RasG12V Cluster Formation

BHK cells were transfected with mGFP-KRasG12V and treated with DMSO, SB590885 (0.2 μM), or sorafenib (10 μM). The trajectories of single mGFP-K-RasG12V molecules diffusing on the plasma membrane were tracked and analyzed.

(A) Representative trajectories of single K-RasG12V molecules that show periods of free diffusion and transient immobilization, which are marked by circles.

(B) More than 750 individual trajectories were analyzed to generate distribution histograms of the duration and radii of all the temporary immobilization events. The duration distributions were fitted by single exponential decay functions to provide the exponential time constants shown.

(C) A summary of the single-molecule imaging analysis of K-RasG12V. Differences between DMSO- and Raf inhibitor-treated cells were assessed using Mann-Whitney U tests, and significant differences are indicated (**$p < 0.01$) (n, the number of occurrences of temporary immobilization events). The exponential time constants derived in (B) were corrected for the photobleaching lifetime of mGFP on the cell surface (= 540 ± 73 ms). The mean radii of immobilization events derived in (B) were corrected for precision of localization as described in the Experimental Procedures. See also Movies S1, S2, and S3.

proteins that assemble into nanoclusters, the clustered fraction, sets the gain for Ras-MAPK signal transmission [3, 6–8, 23], therefore an increase in the Ras clustered fraction will increase ppERK output at any given concentration of Ras.GTP (Figure 7). The change in signal gain is most clearly illustrated by the increased slope of the dose response to EGF observed in BRaf inhibited cells (Figure 7). Our results also account for the increased Raf translocation to the plasma membrane seen in BRaf inhibited cells [12, 13, 15]; although the total amount of Ras.GTP does not change in the presence of Raf inhibitors, the number of Ras nanoclusters, which are the sites for Raf recruitment to the plasma membrane, does increase.

We observed an interesting interaction between Akt and MAPK activity in cells treated with BRaf inhibitors; as MAPK activity increased, pAkt levels decreased. Our results further show that as Ras nanoclusters are crosslinked and occupied by bivalent Raf complexes, p110α association with the plasma membrane is inhibited. The simplest interpretation of these data is that different effectors compete for recruitment to Ras.GTP nanoclusters, such that if a Ras nanocluster is occupied by a Raf, KSR, MEK, ERK complex, then access is denied to PI3K. This phenomenon of effector exclusion is a novel form of pathway crosstalk, not described previously [33], that could contribute to the therapeutic effect of Raf inhibitors. Indeed, we observed reciprocity between elevated ppERK and decreased pAkt in a cohort of K-Ras transformed cancer cell lines treated with BRaf inhibitors. Intriguingly, a recent study has shown that other ATP-competitive kinase inhibitors, such as imatinib, nilotinib, and dasatinib, can also drive Raf dimerization and drive paradoxical activation of MAPK in Ras transformed cells [34]. It seems probable that the mechanism for the effect of imatinib and these other weak Raf inhibitors will be the same as we have described here for BRaf inhibitors.

The weaker effect of Raf inhibitors on H-Ras.GTP nanoclusters is an important result that merits further consideration. The differential sensitivity of H-Ras.GTP and K-Ras.GTP nanoclusters crosslinking by stabilized Raf dimers may in part be explained by earlier work showing that whereas K-Ras.GTP nanoclusters efficiently retain Raf recruited from the cytosol, H-Ras.GTP nanoclusters do not [18]. However, the FLIM-FRET results infer that Raf dimers are present in H-Ras.GTP nanoclusters and in turn significantly abrogate PI3K/Akt activation. Raf dimers are, however, unable to enhance H-Ras nanoclustering. The molecular mechanism that underlies H-Ras nanoclustering is quite different from that for K-Ras, and although a molecular scaffold, galectin-1, is involved, this does not operate by crosslinking H-Ras.GTP molecules but by stabilizing a conformation of H-Ras.GTP that is favorable for nanocluster assembly [35–37]. Whatever the reason for the failure of the dimers to enhance HG12V nanoclustering, the inability to increase the H-Ras clustered fraction can account for the much weaker activation of MAPK in H-Ras transformed cells treated with BRaf inhibitors.

The spatiotemporal organization of Ras on the plasma membrane endows important emergent properties on signal transmission via the MAPK cascade. We show here that dysregulation of the dynamics of nanocluster assembly is a major

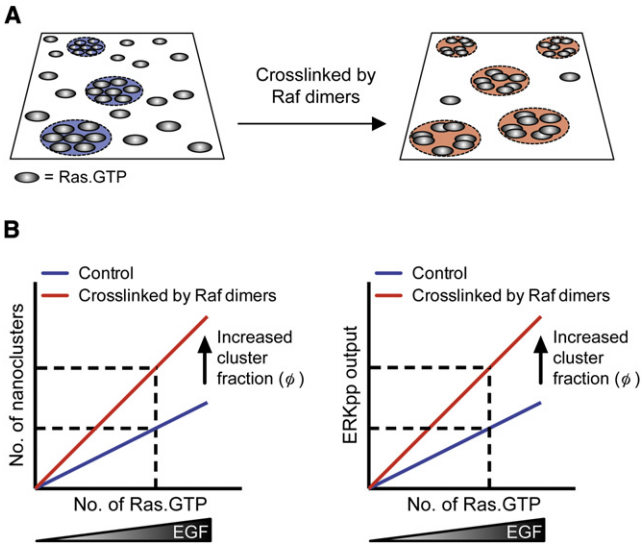


Figure 7. Model of the Effect of BRaf Inhibitors on Ras Spatiotemporal Dynamics

(A) A fixed proportion of K-Ras.GTP molecules (the clustered fraction) assemble into transient signaling nanoclusters (blue circles). BRaf inhibition generates stable Raf dimers that crosslink K-Ras.GTP (or N-Ras.GTP) molecules facilitating nanocluster formation (red circles).

(B) Nanoclusters output fixed quanta of ppERK and total ppERK system response is therefore the aggregated output from all signaling nanoclusters. The consequences of Raf dimers facilitating nanocluster formation are to increase the Ras clustered fraction ($\phi$) such that a greater number of nanoclusters are assembled at any given Ras.GTP concentration. In turn, the increased number of Ras nanoclusters generates a greater aggregated ppERK output from the plasma membrane at each Ras.GTP concentration.

consequence of treating cells with BRaf inhibitors that results in divergent consequences for MAPK and PI3K activity. The study identifies perturbation of Ras spatiotemporal dynamics as the molecular mechanism driving paradoxical activation of the MAPK cascade by BRaf inhibitors, but also suggests that these same dynamics may represent a novel target for future therapeutic intervention.

## Experimental Procedures

### Cell Culture

Baby hamster kidney (BHK) cells were maintained in Dulbecco's modified Eagle medium (DMEM) (GIBCO) supplemented with 10% donor calf serum (DCS). Chinese hamster ovarian cells (CHO) and A549 cells were maintained in Ham's F-12K medium (ATCC) supplemented with 10% fetal bovine serum (FBS). HES and MDA-MB-231 cells were maintained in DMEM (GIBCO) supplemented with 10% FBS. HEC-1a, Ishikawa, and ESS-1 cells were maintained in McCoy's 5A (GIBCO), MEM (GIBCO), and RPMI-1640 (ATCC), respectively, supplemented with 10% FBS. All cell lines were grown at 37°C in 5% CO2. To generate stable cell lines, we transfected BHK cells with mGFP-RasG12V constructs in the pEF6/V5-His-Topo plasmid (Invitrogen) using Lipofectamine (Invitrogen) according to the manufacturer's instructions. Following an overnight incubation, GFP-Ras expressing cells were isolated using fluorescence-activated cell sorting (FACS) and maintained in BHK medium containing 20 μg/mL blasticidin (Sigma Aldrich).

### Fluorescence Lifetime Imaging-Fluorescence Resonance Energy Transfer Microscopy

FLIM-FRET experiments were carried out using a lifetime fluorescence imaging attachment (Lambert Instruments, The Netherlands) on an inverted microscope [18]. BHK cells transiently expressing mGFP-tagged protein (donor), alone or with mRFP-tagged protein (acceptor) (using a 1:1 ratio of plasmid DNA), were prepared as indicated in each experiment. The samples were excited using a sinusoidally modulated 3 W 470 nm light-emitting diode at 40 MHz under epi-illumination. Fluorescein was used as a lifetime reference standard. Cells were imaged with a Plan Apo 60X 1.40 oil objective using an appropriate GFP filter set. The phase and modulation were determined from 12 phase settings using the manufacturer's software. Resolution of two lifetimes in the frequency domain was performed using a graphical method [38] mathematically identical to global analysis algorithms [39, 40]. The analysis yields the mGFP lifetime of free mGFP donor ($=\tau_1$), the mGFP lifetime in donor acceptor complexes ($=\tau_2$), and estimates the fraction of mGFP in donor-acceptor complexes ($\alpha$). FRET efficiency is then calculated as $1 - \tau_2/\tau_1$. FLIM data were averaged on a per-cell basis. To quantify the fraction of mRFP without a functional chromophore, we performed FLIM measurements on BHK cells expressing an mGFP-mRFP fusion protein and obtained a value of $\alpha = 0.35 \pm 0.05$ (mean ± SEM). Our estimates of FRET fractions take this into account.

### EM and Spatial Mapping

Plasma membrane sheets were fixed and labeled with anti-GFP antibody conjugated to 5 nm gold particles as previously described [41, 42]. For bivariate analysis, plasma membrane sheets were labeled with anti-mRFP antibody conjugated to 2 nm gold particles and anti-GFP antibody conjugated to 6 nm gold particles. Digital images of the immunogold-labeled plasma membrane sheets were taken in a transmission electron microscope. Intact 1 $\mu m^2$ areas of the plasma membrane sheet were identified using ImageJ, and the (x, y) coordinates of the gold particles were determined [41, 42]. K-functions [43] were calculated and standardized on the 99% or 95% confidence interval (C.I.) for univariate or bivariate functions, respectively [41, 42, 44]. Bootstrap tests to examine differences between replicated point patterns were constructed exactly as described previously [8, 44], and statistical significance was evaluated against 1,000 bootstrap samples. Extraction of clustered fractions and estimated number of gold particles per cluster were extracted from the spatial point patterns as previously described [8, 44]. Conversion of numbers of gold particles per cluster to estimated number of Ras proteins per cluster used the measured capture ratio of the anti-GFP antibody [8, 44].

### Western Blotting

Cells were washed in cold phosphate-buffered saline (PBS) and subjected to detergent lysis in a buffer containing 50 mM TrisCl (pH 7.5), 75 mM NaCl, 25 mM NaF, 5 mM $MgCl_2$, 5 mM EGTA, 1 mM dithiothreitol, 100 μM $NaVO_4$, and 1% Nonidet P40 plus protease inhibitors. SDS-PAGE and immunoblotting with the specified antibody were performed using 20 μg of each lysate. Signal was detected by enhanced chemiluminescence (SuperSignal; Pierce, Thermo Fisher Scientific, Rockford, IL) and imaged using a FluorChemQ (Alpha Inotech, San Leandro, CA). Quantification of intensities was performed using FluorChemQ software.

### Statistical Analysis

Prism (Version 5.0c, GraphPad Software) was used for one-way ANOVA testing.

### Video Tracking

SFVT was performed on BHK cells transiently expressing mGFP-KRasG12V, as described previously [27]. To analyze and identify temporary immobilization periods (TIMPs) of mGFP-KRasG12V, we used the method developed by Sahl et al. [45]. The parameters used for the present analysis were as follows: detection diameter 120 nm; threshold for detection = 3 frames; smoothing = 2 frames. We were unable to directly obtain the distributions of the durations for diffusing events from the experiments because the trajectory lengths (determined by photobleaching) were generally too short to include two immobilization events and thus measure the duration of diffusion. However, by assuming a simple exponential distribution of mobile periods (as we observed for the TIMPs), we calculated the lifetime for diffusing periods from the time fraction and the exponential lifetime of the temporary immobilization. If:

$[M]$ = time fraction of the mobile period,

$[I]$ = time fraction of the immobile period

$\tau_M$ = exponential lifetime of the mobile period

$\tau_I$ = exponential lifetime of the immobile period

$$\text{then : } \frac{[M]}{\tau_M} = \frac{[I]}{\tau_I}$$

$$\tau_M = \frac{[M]}{[I]}\tau_I$$

The size of an immobilized site was obtained as the SD of the distance between the average position during the immobilization period and the position determined for each image frame (during immobilization). This value was corrected for the precision of localization (determination of the position of single molecules), which was convoluted in the experimental measurements. The localization error (Gaussian) was 19.8 (±0.48) nm. The radius after subtracting localization error was obtained by the following equation:

$$\left[(\text{estimated radius})^2 - (19.8)^2\right]^{1/2}$$

To determine the localization error for mGFP, we attached mGFP to and immobilized it on a coverslip. From the determined coordinates of single molecules, the distance between the determined positions in consecutive frames (= the step size) was calculated for all the obtained trajectories. The distribution of the step size x (in the x direction) was obtained and fitted by the following equation:

$$f(X) = \frac{X}{2\sigma_{mGFP}^2}\exp\left(-\frac{X^2}{4\sigma_{mGFP}^2}\right)$$

where $\sigma_{mGFP}$ is the fitting parameter, giving the localization error. The error for this distribution can be estimated by the fitting error for the 68.3% confidence limit, which was 0.47 nm.

## Supplemental Information

Supplemental Information includes four figures, one table, and three movies and can be found with this article online at doi:10.1016/j.cub.2012.03.067.

## Acknowledgments

This work was supported the Cancer Prevention and Research Institute of Texas (CPRIT RP100483). J.F.H. is the current incumbent of the John S. Dunn Distinguished University Chair. The iCeMS of Kyoto University is supported by World Premier International Research Center Initiative (WPI) of the Japanese government (MEXT). R.M. and S.J.H. declare that employees at the Institute of Cancer Research may receive remuneration through the "rewards to inventors scheme" for any product that is commercialized.

Received: October 28, 2011
Revised: February 10, 2012
Accepted: March 20, 2012
Published online: May 3, 2012

## References

1. Kusumi, A., Suzuki, K.G., Kasai, R.S., Ritchie, K., and Fujiwara, T.K. (2011). Hierarchical mesoscale domain organization of the plasma membrane. Trends Biochem. Sci. *36*, 604–615.
2. Levental, I., Grzybek, M., and Simons, K. (2010). Greasing their way: lipid modifications determine protein association with membrane rafts. Biochemistry *49*, 6305–6316.
3. Tian, T., Harding, A., Inder, K., Plowman, S., Parton, R.G., and Hancock, J.F. (2007). Plasma membrane nanoswitches generate high-fidelity Ras signal transduction. Nat. Cell Biol. *9*, 905–914.
4. Hancock, J.F. (2006). Lipid rafts: contentious only from simplistic standpoints. Nat. Rev. Mol. Cell Biol. *7*, 456–462.
5. Simons, K., and Toomre, D. (2000). Lipid rafts and signal transduction. Nat. Rev. Mol. Cell Biol. *1*, 31–39.
6. Kholodenko, B.N., Hancock, J.F., and Kolch, W. (2010). Signalling ballet in space and time. Nat. Rev. Mol. Cell Biol. *11*, 414–426.
7. Harding, A.S., and Hancock, J.F. (2008). Using plasma membrane nanoclusters to build better signaling circuits. Trends Cell Biol. *18*, 364–371.
8. Plowman, S.J., Muncke, C., Parton, R.G., and Hancock, J.F. (2005). H-ras, K-ras, and inner plasma membrane raft proteins operate in nanoclusters with differential dependence on the actin cytoskeleton. Proc. Natl. Acad. Sci. USA *102*, 15500–15505.
9. Poulikakos, P.I., and Rosen, N. (2011). Mutant BRAF melanomas—dependence and resistance. Cancer Cell *19*, 11–15.
10. Joseph, E.W., Pratilas, C.A., Poulikakos, P.I., Tadi, M., Wang, W., Taylor, B.S., Halilovic, E., Persaud, Y., Xing, F., Viale, A., et al. (2010). The RAF inhibitor PLX4032 inhibits ERK signaling and tumor cell proliferation in a V600E BRAF-selective manner. Proc. Natl. Acad. Sci. USA *107*, 14903–14908.
11. Flaherty, K.T., Puzanov, I., Kim, K.B., Ribas, A., McArthur, G.A., Sosman, J.A., O'Dwyer, P.J., Lee, R.J., Grippo, J.F., Nolop, K., and Chapman, P.B. (2010). Inhibition of mutated, activated BRAF in metastatic melanoma. N. Engl. J. Med. *363*, 809–819.
12. Heidorn, S.J., Milagre, C., Whittaker, S., Nourry, A., Niculescu-Duvas, I., Dhomen, N., Hussain, J., Reis-Filho, J.S., Springer, C.J., Pritchard, C., and Marais, R. (2010). Kinase-dead BRAF and oncogenic RAS cooperate to drive tumor progression through CRAF. Cell *140*, 209–221.
13. Hatzivassiliou, G., Song, K., Yen, I., Brandhuber, B.J., Anderson, D.J., Alvarado, R., Ludlam, M.J., Stokoe, D., Gloor, S.L., Vigers, G., et al. (2010). RAF inhibitors prime wild-type RAF to activate the MAPK pathway and enhance growth. Nature *464*, 431–435.
14. Poulikakos, P.I., Zhang, C., Bollag, G., Shokat, K.M., and Rosen, N. (2010). RAF inhibitors transactivate RAF dimers and ERK signalling in cells with wild-type BRAF. Nature *464*, 427–430.
15. Anderson, D.J., Durieux, J.K., Song, K., Alvarado, R., Jackson, P.K., Hatzivassiliou, G., and Ludlam, M.J. (2011). Live-cell microscopy reveals small molecule inhibitor effects on MAPK pathway dynamics. PLoS ONE *6*, e22607.
16. Wilhelm, S.M., Carter, C., Tang, L., Wilkie, D., McNabola, A., Rong, H., Chen, C., Zhang, X., Vincent, P., McHugh, M., et al. (2004). BAY 43-9006 exhibits broad spectrum oral antitumor activity and targets the RAF/MEK/ERK pathway and receptor tyrosine kinases involved in tumor progression and angiogenesis. Cancer Res. *64*, 7099–7109.
17. Whittaker, S., Ménard, D., Kirk, R., Ogilvie, L., Hedley, D., Zambon, A., Lopes, F., Preece, N., Manne, H., Rana, S., et al. (2010). A novel, selective, and efficacious nanomolar pyridopyrazinone inhibitor of V600EBRAF. Cancer Res. *70*, 8036–8044.
18. Plowman, S.J., Ariotti, N., Goodall, A., Parton, R.G., and Hancock, J.F. (2008). Electrostatic interactions positively regulate K-Ras nanocluster formation and function. Mol. Cell. Biol. *28*, 4377–4385.
19. Suzuki, K.G., Fujiwara, T.K., Edidin, M., and Kusumi, A. (2007). Dynamic recruitment of phospholipase C gamma at transiently immobilized GPI-anchored receptor clusters induces IP3-Ca2+ signaling: single-molecule tracking study 2. J. Cell Biol. *177*, 731–742.
20. Suzuki, K.G., Fujiwara, T.K., Sanematsu, F., Iino, R., Edidin, M., and Kusumi, A. (2007). GPI-anchored receptor clusters transiently recruit Lyn and G alpha for temporary cluster immobilization and Lyn activation: single-molecule tracking study 1. J. Cell Biol. *177*, 717–730.
21. Nassar, N., Horn, G., Herrmann, C., Scherer, A., McCormick, F., and Wittinghofer, A. (1995). The 2.2 A crystal structure of the Ras-binding domain of the serine/threonine kinase c-Raf1 in complex with Rap1A and a GTP analogue. Nature *375*, 554–560.
22. Kenworthy, A.K. (2007). Nanoclusters digitize Ras signalling. Nat. Cell Biol. *9*, 875–877.
23. Harding, A., and Hancock, J.F. (2008). Ras nanoclusters: combining digital and analog signaling. Cell Cycle *7*, 127–134.
24. Mor, A., and Philips, M.R. (2006). Compartmentalized Ras/MAPK signaling. Annu. Rev. Immunol. *24*, 771–800.
25. Chiu, V.K., Bivona, T., Hach, A., Sajous, J.B., Silletti, J., Wiener, H., Johnson, R.L., 2nd, Cox, A.D., and Philips, M.R. (2002). Ras signalling on the endoplasmic reticulum and the Golgi. Nat. Cell Biol. *4*, 343–350.
26. Inder, K., Harding, A., Plowman, S.J., Philips, M.R., Parton, R.G., and Hancock, J.F. (2008). Activation of the MAPK module from different spatial locations generates distinct system outputs. Mol. Biol. Cell *19*, 4776–4784.
27. Murakoshi, H., Iino, R., Kobayashi, T., Fujiwara, T., Ohshima, C., Yoshimura, A., and Kusumi, A. (2004). Single-molecule imaging analysis of Ras activation in living cells. Proc. Natl. Acad. Sci. USA *101*, 7317–7322.
28. Hancock, J.F., and Parton, R.G. (2005). Ras plasma membrane signalling platforms. Biochem. J. *389*, 1–11.
29. Hu, J., Yu, H., Kornev, A.P., Zhao, J., Filbert, E.L., Taylor, S.S., and Shaw, A.S. (2011). Mutation that blocks ATP binding creates a pseudokinase stabilizing the scaffolding function of kinase suppressor of Ras, CRAF and BRAF. Proc. Natl. Acad. Sci. USA *108*, 6067–6072.
30. Shalom-Feuerstein, R., Plowman, S.J., Rotblat, B., Ariotti, N., Tian, T., Hancock, J.F., and Kloog, Y. (2008). K-ras nanoclustering is subverted by overexpression of the scaffold protein galectin-3. Cancer Res. *68*, 6608–6616.

31. Tian, T., Plowman, S.J., Parton, R.G., Kloog, Y., and Hancock, J.F. (2010). Mathematical modeling of K-Ras nanocluster formation on the plasma membrane. Biophys. J. *99*, 534–543.
32. Levy, R., Grafi-Cohen, M., Kraiem, Z., and Kloog, Y. (2010). Galectin-3 promotes chronic activation of K-Ras and differentiation block in malignant thyroid carcinomas. Mol. Cancer Ther. *9*, 2208–2219.
33. Mendoza, M.C., Er, E.E., and Blenis, J. (2011). The Ras-ERK and PI3K-mTOR pathways: cross-talk and compensation. Trends Biochem. Sci. *36*, 320–328.
34. Packer, L.M., Rana, S., Hayward, R., O'Hare, T., Eide, C.A., Rebocho, A., Heidorn, S., Zabriskie, M.S., Niculescu-Duvaz, I., Druker, B.J., et al. (2011). Nilotinib and MEK inhibitors induce synthetic lethality through paradoxical activation of RAF in drug-resistant chronic myeloid leukemia. Cancer Cell *20*, 715–727.
35. Belanis, L., Plowman, S.J., Rotblat, B., Hancock, J.F., and Kloog, Y. (2008). Galectin-1 is a novel structural component and a major regulator of h-ras nanoclusters. Mol. Biol. Cell *19*, 1404–1414.
36. Abankwa, D., Gorfe, A.A., Inder, K., and Hancock, J.F. (2010). Ras membrane orientation and nanodomain localization generate isoform diversity. Proc. Natl. Acad. Sci. USA *107*, 1130–1135.
37. Abankwa, D., Gorfe, A.A., and Hancock, J.F. (2007). Ras nanoclusters: molecular structure and assembly. Semin. Cell Dev. Biol. *18*, 599–607.
38. Clayton, A.H., Hanley, Q.S., and Verveer, P.J. (2004). Graphical representation and multicomponent analysis of single-frequency fluorescence lifetime imaging microscopy data. J. Microsc. *213*, 1–5.
39. Verveer, P.J., and Bastiaens, P.I. (2003). Evaluation of global analysis algorithms for single frequency fluorescence lifetime imaging microscopy data. J. Microsc. *209*, 1–7.
40. Esposito, A., Gerritsen, H.C., and Wouters, F.S. (2005). Fluorescence lifetime heterogeneity resolution in the frequency domain by lifetime moments analysis. Biophys. J. *89*, 4286–4299.
41. Hancock, J.F., and Prior, I.A. (2005). Electron microscopic imaging of Ras signaling domains. Methods *37*, 165–172.
42. Prior, I.A., Muncke, C., Parton, R.G., and Hancock, J.F. (2003). Direct visualization of Ras proteins in spatially distinct cell surface microdomains. J. Cell Biol. *160*, 165–170.
43. Ripley, B.D. (1977). Modelling spatial patterns. J. R. Stat. Soc., B *39*, 172–192.
44. Diggle, P.J., Mateu, J., and Clough, H.E. (2000). A comparison between parametric and non-parametric approaches to the analysis of replicated spatial point patterns. Adv. Appl. Probab. *32*, 331–343.
45. Sahl, S.J., Leutenegger, M., Hilbert, M., Hell, S.W., and Eggeling, C. (2010). Fast molecular tracking maps nanoscale dynamics of plasma membrane lipids. Proc. Natl. Acad. Sci. USA *107*, 6829–6834.